Evaluating Modified Diffusion Coefficients for the SST Turbulence Model Using Benchmark Tests

Scott M. Murman

Scott.M.Murman@nasa.gov

NASA Ames Research Center, Moffett Field, CA, USA

Abstract

Empirical modification of the diffusion coefficients for the shear-stress-transport (SST) turbulence model is presented against experimental data for a suite of model test problems. The modified form improves the prediction of mean flow and turbulent quantities at the edge of a free shear layer without significantly disrupting established correlations. The suite of benchmark cases illuminates turbulence modeling trends across a diverse range of flows, encompassing different physical mechanisms. This diversity and automation improves model validation, code regression testing, and the development of novel models.

1 Introduction

NASA is currently analyzing several configurations in which the generation, convection, and impingement of free shear layers plays an important role in predicting vehicle performance. Figure 1 contains two examples: the separated boundary layer and wake from the Multi Purpose Crew Vehicle, which impact the vehicle dynamic stability and performance of the parachute system, and plumes from the Orion Launch Abort Vehicle abort motors, which impinge upon the aft body of the vehicle affecting the static stability and local heating. To address the predictive capability of Computational Fluid Dynamics (CFD) for these types of complex flows, a database of model problems and associated turbulent experimental results is being catalogued. This catalogue includes free shear and wall-bounded flows, diffusers, shock-boundary-layer interaction, wall jets, *etc.*

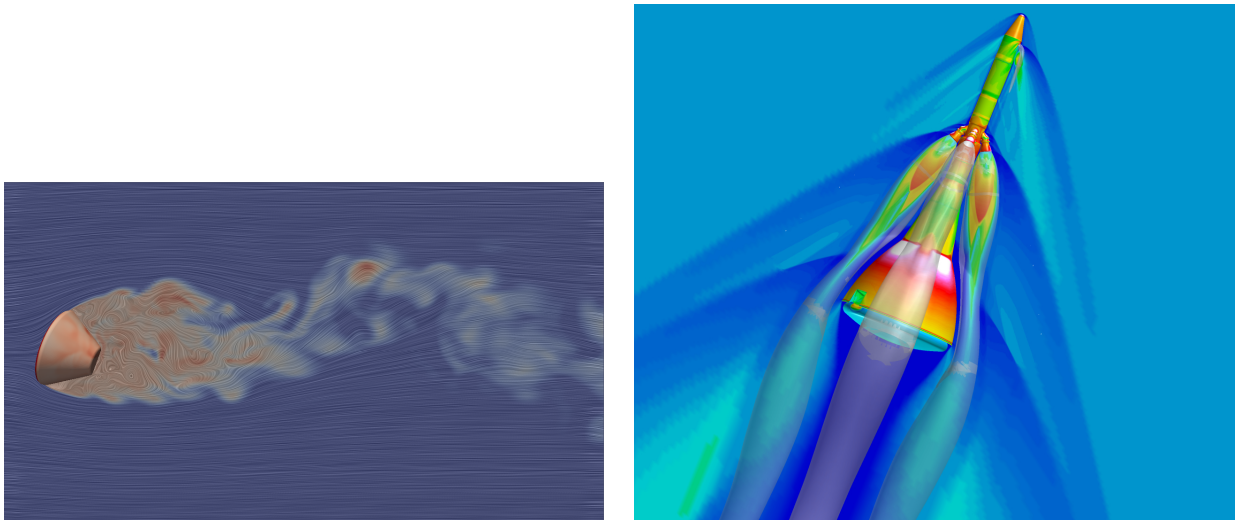

(**a**) Multi Purpose Crew Vehicle (**b**) Orion Launch Abort Vehicle

Figure 1: Example computed flowfields highlighting the significance of free shear-layers in predicting vehicle performance. Launch Abort Vehicle image courtesy Tom Booth, NASA Johnson Space Center.

Bardina *et al.*[1] demonstrated the utility of benchmark test cases in evaluating turbulence model performance, building from specialized CFD solvers for the boundary-layer equations and other self-similar systems. The database described here includes many of the benchmark cases from [1], along with several additions, and is initially aimed at evaluating general-purpose production Navier-Stokes CFD solvers, such as OVERFLOW-2[2]. Recently, the Turbulence Model Benchmarking Working Group (TMBWG) formed a website for turbulence model verification and validation[3]. The initial goal of the TMBWG is to verify whether a specific model implementation is correct by comparison against previously verified implementations of the same model on benchmark cases. While there is overlap between the TMBWG approach and the current work, the focus of the current turbulence model catalogue is sufficiently different to require a separate effort. Rather than evaluating specific models against similar implementations to verify correctness, the current suite aims to evaluate models which continually change with time, due to enhancements or implementation changes, against a database of experimental results. This effort is aimed not only at validation, but also regression testing code changes, and development of new modeling approaches. As a motivating example, there are numerous turbulence model "corrections" which adjust a baseline turbulence model in certain situations. Using OVERFLOW-2 as an example, the following run-time turbulence model corrections are available for two-equation models: compressibility, temperature, streamline curvature(2), hybrid-RANS/DES(3), and wall functions. Complex flow simulations,

such as those in Fig. 1, commonly use one or more of these corrections (cf. Childs *et al.*[4]), however understanding how these nonlinear corrections perform in isolation across a range of benchmark problems, much less in combination, is often undocumented. The current database provides a solution to this issue, as well as a tool to improve both the corrections and the baseline models themselves. An empirical modification of the shear-stress-transport (SST) turbulence model[5], developed using the database, is included in this work as an example of a model improvement for the prediction of mean flow and turbulent quantities across a free shear layer.

The current work concurrently describes the performance of the modified SST model and provides an overview of the benchmark cases by sampling the turbulent model problems database. The paper first provides brief background information on the criteria used to select benchmark cases and the SST turbulence model itself. The performance of the baseline and modified SST model are then presented for free-shear, wall-bounded, and adverse-pressure-gradient flows. Lastly, a summary of the work is presented.

2 Background

There are numerous CFD validation cases in the literature, and criteria are necessary to downselect those for turbulence model benchmarking. The criteria used here include that, at a minimum, both experimental mean flow and turbulent velocity fluctuation data are available. Preference is given to cases with a simple well-defined geometry. Lastly, cases do not require modeling of laminar and transitional flow regimes, as is common with airfoil and cylinder configurations, and similarly do not require artificial "tripping" of the boundary layer to promote transition. The following comprises the current list of turbulence model benchmark cases,

- Mixing layer (varying convective Mach number)
- Planar Wake
- Planar Jet
- Axisymmetric Jet (varying jet exit Mach number)
- Zero-pressure-gradient Flat Plate (low and high Mach number)
- Channel Flow
- Wall Jet (quiescent and co-flowing freestream)

- Adverse-pressure-gradient Boundary Layer (mild and strong)
- Planar Diffuser
- Axisymmetric Diffuser
- Axisymmetric Transonic Bump
- Backward-facing Step
- Jet-in-crossflow
- Isotropic Turbulence and Decay
- Fundamental Aeronautics Investigation of The Hill (FAITH)

This list is expected to grow and be refined as improved datasets become available. The ultimate goal is to release the suite to the general community.

The current work does not present computed results for the complete catalogue of cases. The chosen cases are intended to provide an overview of the capability, and highlight the modified SST diffusion coefficients for a range of flow physics. The computed cases presented here all correspond to low-speed flows to simplify the discussion. To facilitate automatic testing and mesh refinement studies, the mesh generation for each case is performed using the Chimera Grid Tools scripting[6]. While the focus of the current work is the OVERFLOW-2 solver, none of the current configurations use overset meshes, and hence are straightforward to adapt to other solvers. Mesh resolution studies were performed for all cases, and all computed results were converged to a steady-state with "machine zero" residual. Details of these numerical studies are omitted for brevity. All simulations use the central differencing with matrix dissipation option in OVERFLOW-2 for the convective terms, with default values for all other numerical options. The *ad hoc* turbulent eddy viscosity limiting in OVERFLOW-2 (`MUT_LIMIT`) is disabled for all simulations.

Several similar simulations of a turbulent jet expelling into a quiescent reservoir are presented in this work (cf. Fig. 2). These flows develop into self-similar profiles, and the details of the developing flow region are not considered. Each uses a domain of dimension $400b$ x $200b$, with b being the extent of the jet (height or radius), and a jet exit Mach number of $M_j = 0.2$. The jet is imposed as a step profile, with the actual nozzle geometry ignored. The self-similar region is determined from analysis of the jet spreading and decay rates.

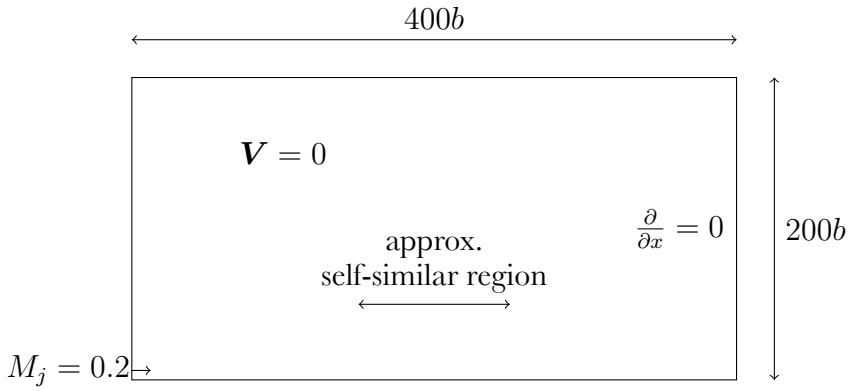

Figure 2: Computational domain for jet cases. b is the extent of the jet (height or radius).

The SST turbulence model is a two-equation model based on the k-ω equations,

$$\begin{aligned}
\frac{D\rho k}{Dt} &= \tau_{ij}\frac{\partial u_i}{\partial x_j} - \beta^*\rho\omega k + \frac{\partial}{\partial x_j}\left[\left(\mu + \sigma_k\mu_t\right)\frac{\partial k}{\partial x_j}\right] \\
\frac{D\rho\omega}{Dt} &= \frac{\gamma}{\nu_t}\tau_{ij}\frac{\partial u_i}{\partial x_j} - \beta\rho\omega^2 + \frac{\partial}{\partial x_j}\left[\left(\mu + \sigma_\omega\mu_t\right)\frac{\partial \omega}{\partial x_j}\right] + 2\rho\left(1-F_1\right)\frac{\sigma_\omega}{\omega}\frac{\partial k}{\partial x_j}\frac{\partial \omega}{\partial x_j} \\
\mu_t &= \frac{\rho k}{\omega} \qquad\qquad \rho\tau_{ij} = 2\mu_t S_{ij}
\end{aligned} \tag{1}$$

where S_{ij} is the mean strain rate, and τ_{ij} is the turbulent Reynolds stress.* The closure coefficients for an inner (subscript 1) and outer layer (subscript 2) are,

$$\begin{aligned}
\beta^* = 0.09, \quad \kappa = 0.41 \\
\sigma_{k1} = 0.85, \quad \sigma_{\omega1} = 0.5, \quad \beta_1 = 0.0750, \quad \gamma_1 = \beta_1/\beta^* - \sigma_{\omega1}\kappa^2/\sqrt{\beta^*} \\
\sigma_{k2} = 1.0, \quad \sigma_{\omega2} = 0.856, \quad \beta_2 = 0.0828, \quad \gamma_2 = \beta_2/\beta^* - \sigma_{\omega2}\kappa^2/\sqrt{\beta^*}
\end{aligned} \tag{2}$$

and F_1 the blending function between inner and outer layers (*cf.* [5] for complete details).†

*OVERFLOW-2 uses a pseudo-compressible formulation for the turbulence equations.

†OVERFLOW-2 uses a different $\sigma_{\omega1}$ than the original SST formulation.

3 Free Shear Flows

3.1 Axisymmetric Jet

The diffusion modifications to the SST model are motivated by the simulation results for an axisymmetric jet. Predicting this model flow is a building block to the more complex nozzle flows common in flight vehicles. Figure 3 presents computed results compared to the experimental data of Hussein *et al.*[7] for mean flow and turbulent fluctuations. The standard model overpredicts the Reynolds stress in the center of the self-similar profile, and underpredicts at the edges of the shear layer. As the Reynolds stress and mean flow are coupled in a self-similar flow, the computed mean-flow velocity profile likewise shows a discrepancy compared to the experimental data at the edge of the shear layer. In this figure, and the ones which follow, three axial stations are plotted from each simulation to demonstrate the computed profiles are self-similar. The predictions are improved by increasing the outer-layer diffusion coefficients over the standard values, while keeping the ratio σ_k/σ_ω roughly the same, and without modifying the production. The modified SST outer layer coefficients are,

$$\sigma_{k2} = 2.0, \quad \sigma_{\omega 2} = 1.5, \quad \beta_2 = 0.0828, \quad \gamma_2 = C_{\epsilon 1} - 1.0 = 0.44, \tag{3}$$

with the computed results included in Fig. 4. Poroseva and Bézard[8] and Cazalbou *et al.*[9] similarly analyze tailoring of the diffusion coefficients for free shear flows for the k-ϵ model. The current modifications are considered purely empirical corrections, though just as theoretical observations often lead to improved models, so can numerical experiments and empirical observations lead to improved theoretical foundations. Note that for a free shear flow, such as the axisymmetric jet, the inner layer of the SST model is not active. The modified diffusion causes the peak turbulent eddy viscosity to diffuse outwards towards the edges of the shear layer, likewise improving the prediction of the mean velocity at the edges of the profile. The predicted turbulent kinetic energy is also in good agreement with the experimental data. As will be shown, since the SST model uses two layers, the calibration of the model for wall-bounded flows is not overly sensitive to these changes in the outer layer.

3.2 Planar Mixing Layer

Given the improved predictions for the target application of an axisymmetric jet, the behavior of the modified diffusion coefficients for a broader range of free shear flows is investigated. The computed results for a planar mixing layer are compared against the experimental data of Bell and

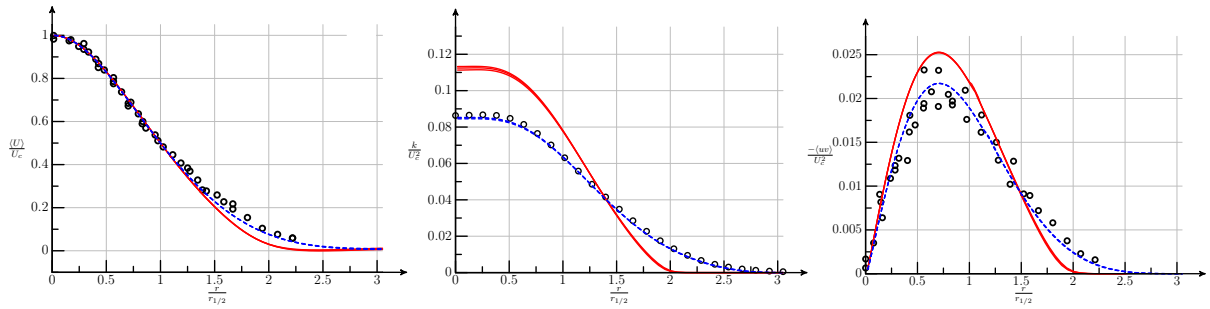

(**a**) Mean Velocity (**b**) Turb. Kinetic Energy (**c**) Reynolds Stress

Figure 3: Computed results for an axisymmetric jet ($Re_j = 10^4$). Symbols, experimental data from Hussein *et al.*[7]. Solid lines, computed results of standard SST model (Eqn. 2). Dashed lines, computed results of modified SST model (Eqn. 3).

Mehta[10] in Fig. 4. As with the axisymmetric jet results, the modified diffusion improves the prediction of Reynolds stress at the edges of the shear layer, which drives a corresponding improvement in the mean flow velocity profile. Here the predicted peak turbulent kinetic energy is lower than the experimental data. This is consistent with DNS results[11], and may indicate a non-unique self-similar flow driven by differences in the initial conditions.

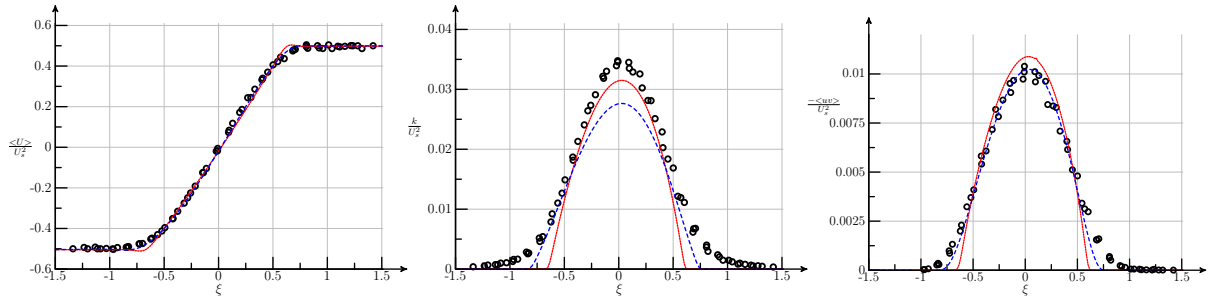

(**a**) Mean Velocity (**b**) Turb. Kinetic Energy (**c**) Reynolds Stress

Figure 4: Computed results for a planar mixing layer. Mixing layer velocity ratio is 0.6, and the convective Mach number is 0.06. Symbols, experimental data from Bell and Mehta[10]. ξ is the scaled distance across the shear layer (cf. [10]). Solid lines, computed results of standard SST model (Eqn. 2). Dashed lines, computed results of modified SST model (Eqn. 3).

3.3 Planar Jet

Simulations of a planar jet are compared to the experimental data of Gutmark and Wygnanski[12] in Fig. 5. Similar to the previous examples, the increased model diffusion coefficients improve the

predictions of both Reynolds stress and mean velocity at the edge of the shear layer. Experimental turbulent kinetic energy data is not included for this case. Neither model achieves true self-similarity at the location of maximum Reynolds stress for this case, as can be seen in the variation of the computed results with axial distance. The cause of this behavior is being investigated, however the qualitative trends of the diffusion coefficient modifications as the flow approaches self-similarity are clear.

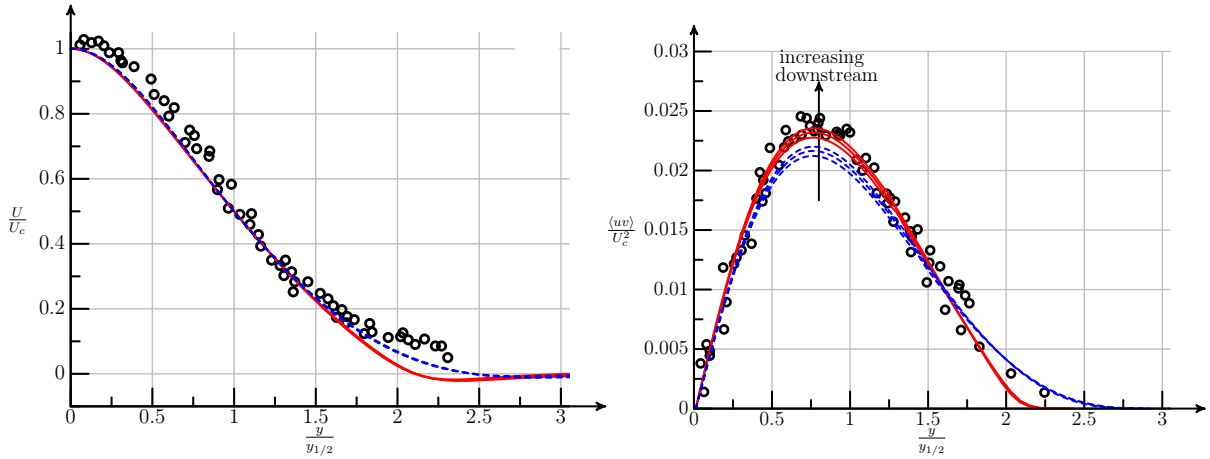

(**a**) Mean Velocity (**b**) Reynolds Stress

Figure 5: Computed results for a planar jet ($Re_j = 10^4$). Symbols, experimental data from Gutmark and Wygnanski[12]. Solid lines, computed results of standard SST model (Eqn. 2). Dashed lines, computed results of modified SST model (Eqn. 3).

Table 1 contains the computed spreading rates in the self-similar region for both the axisymmetric- and planar-jet simulations. The modified diffusion model decreases the predicted spreading rate in both cases. Consistent with previous investigations, the models both predict a greater spreading rate for the axisymmetric jet, which is inconsistent with the experimental data. Use of Pope's vortex stretching parameter[13], or similar, to correct this deficiency in the SST model is an area of future research.

Method	Axisymmetric Jet	Planar Jet
Baseline	2.0	1.6
Modified	1.75	1.5

Table 1: Computed jet spreading rate.

4 Wall-bounded Flows

4.1 Zero-Pressure-Gradient Flat Plate

The computed results using the standard and modified SST model for a zero-pressure-gradient turbulent flat plate are presented in Fig. 6. The simulated flow undergoes a numerical transition from the leading edge, approaching a fully developed turbulent flow as the local Reynolds number increases down the length of the plate. Both forms of the SST model are in good agreement with the experimental skin friction data in the fully developed turbulent regime, and reproduce the viscous sub-layer and log-law regions of the velocity profile. Appropriate smooth-wall high Reynolds number data for the turbulent Reynolds stress is still being sought.

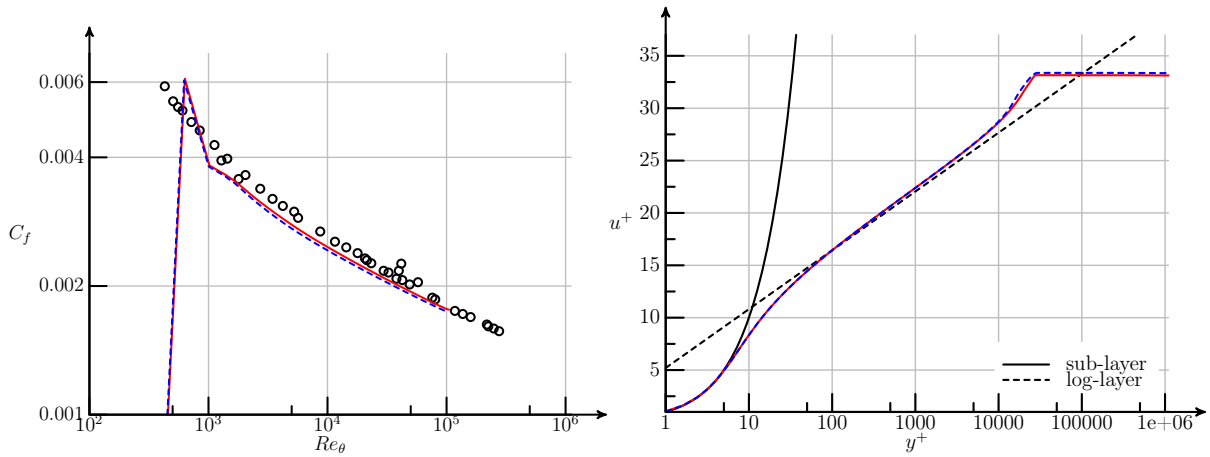

(**a**) Skin Friction (**b**) Velocity Profile

Figure 6: Computed results for a zero-pressure-gradient flat plate ($M_\infty = 0.2$, Re_L =100 x 10^6). Symbols, experimental data from Watson *et al.*[14]. Computed velocity profiles at $Re_\theta \approx 90000$. Solid lines, computed results of standard SST model (Eqn. 2). Dashed lines, computed results of modified SST model (Eqn. 3).

4.2 Planar Wall Jet

Given the computed results for the modified SST model for jet flows and a wall-bounded flow, a natural extension is to investigate the performance for a wall-bounded jet flow into a quiescent reservoir. Figure 7 presents comparisons between the simulations and the experiment of Eriksson *et al.*[15] for both mean flow and turbulent quantities. The modified diffusion coefficients do improve the predictions of mean flow velocity and Reynolds stress at the edge of the shear layer, at the expense of the turbulent kinetic energy, which is consistent with the previous computed results. Both

simulated results predict a rise in Reynolds stress at the inflection point of the mean velocity profile which is not present in the experimental data. The cause of this discrepancy is being investigated.

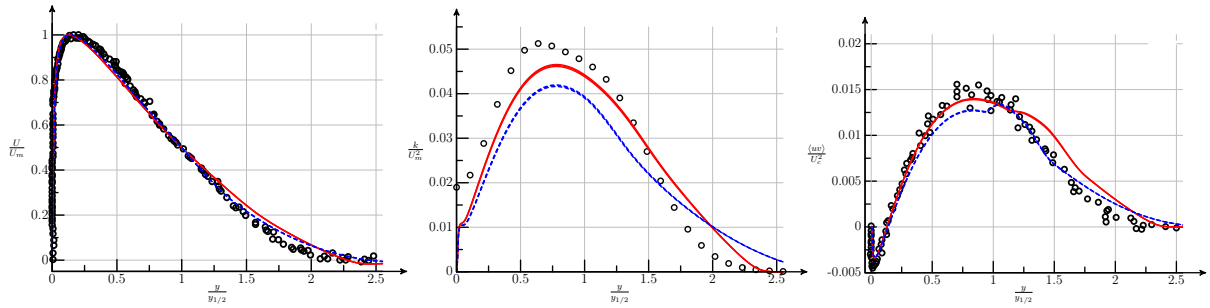

(**a**) Mean Velocity (**b**) Turb. Kinetic Energy (**c**) Reynolds Stress

Figure 7: Computed results for a planar wall jet ($Re_j = 10^3$). Symbols, experimental data from Eriksson *et al.*[15]. The experimental turbulent kinetic energy is determined from regression fits to the velocity fluctuation data using $f(x) = (a_0 + a_2x^2 + a_4x^4 + a_6x^6)\, e^{-bx^2}$. The experimental spanwise turbulent velocity fluctuation is assumed as $\langle ww \rangle = \frac{1}{2}(\langle uu \rangle + \langle vv \rangle)$. Solid lines, computed results of standard SST model (Eqn. 2). Dashed lines, computed results of modified SST model (Eqn. 3).

5 Adverse Pressure Gradient Flows

5.1 Mild Adverse Pressure Gradient

The planar diffuser of Samuel and Joubert[16] is simulated, providing a mild adverse pressure gradient which is steadily increasing along the length of the diffuser (cf. Fig. 8). The computational domain is extended beyond the final experimental measurement station to avoid corrupting the measurements by application of the numerical boundary conditions. This causes the computed flow to eventually separate. Mean flow and turbulent data are taken relative to the horizontal wall, and presented in Fig. 9. There is little to distinguish the computed mean flow velocity profiles using the standard and modified diffusion coefficients, and neither prediction is in strong agreement with the experimental data. These observations are consistent with the computed results originally presented in [17]. The computed turbulent velocity fluctuations are in poor agreement, and do not even reproduce the qualitative trends of the experimental data. The computed peak kinetic energy and Reynolds stress increases with distance traveled, whereas the experimental peak dampens. Unlike the previous benchmark cases, here the increased diffusion counter-intuitively decreases the spreading of the Reynolds stress at the edge of the shear layer.

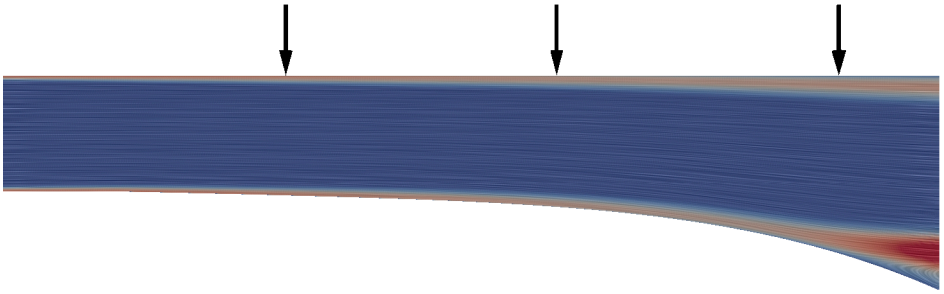

Figure 8: Computed results for a mild adverse pressure gradient ($M_\infty = 0.2$, $Re/L = 1.7\text{x}10^6 m^{-1}$). Flowfield colored by turbulent kinetic energy and line-integral convolution of the velocity field for modified SST model (Eqn. 3). Experimental measurement stations noted by arrows.

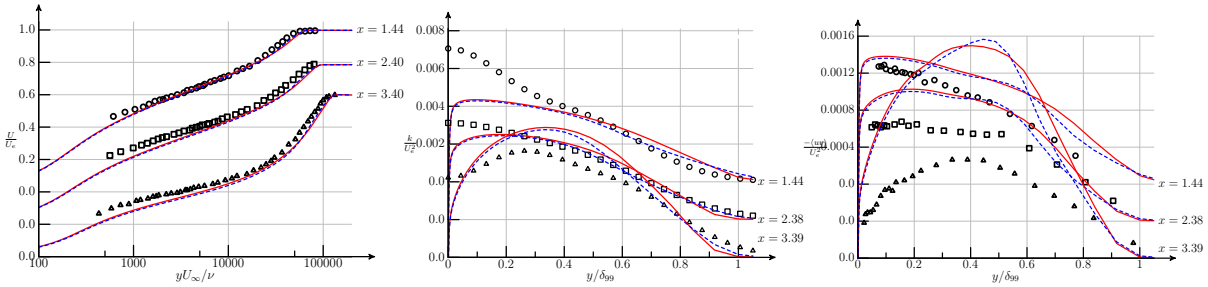

(**a**) Mean Velocity (**b**) Turb. Kinetic Energy (**c**) Reynolds Stress

Figure 9: Computed results for a mild adverse pressure gradient ($M_\infty = 0.2$, $Re/L = 1.7\text{x}10^6 m^{-1}$). Symbols, experimental data from Samuel and Joubert[16]. The experimental turbulent kinetic energy is determined from regression fits to the velocity fluctuation data using $f(x) = (a_0 + a_2x^2 + a_4x^4 + a_6x^6)\, e^{-bx^2}$. Solid lines, computed results of standard SST model (Eqn. 2). Dashed lines, computed results of modified SST model (Eqn. 3).

5.2 Planar Diffuser

The next benchmark case builds on the previous mild adverse pressure gradient, by inducing a large separation region in the planar diffuser studied experimentally by Buice and Eaton[18] (cf. Fig. 10). The computed mean flow and Reynolds stress are presented in Fig. 11. Though the mean flow predictions are in reasonable agreement with the experimental data, both models do overpredict the magnitude of the Reynolds stress in the separated region. However, the modified diffusion does not significantly degrade the performance relative to the standard implementation.

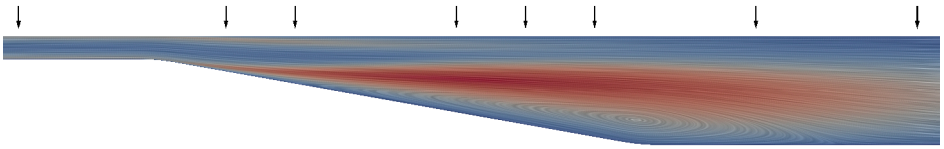

Figure 10: Computed results for a planar diffuser ($Re_H = 20{,}000$). Flowfield colored by turbulent kinetic energy and line-integral convolution of the velocity field for modified SST model (Eqn. 3). Experimental measurement stations noted by arrows.

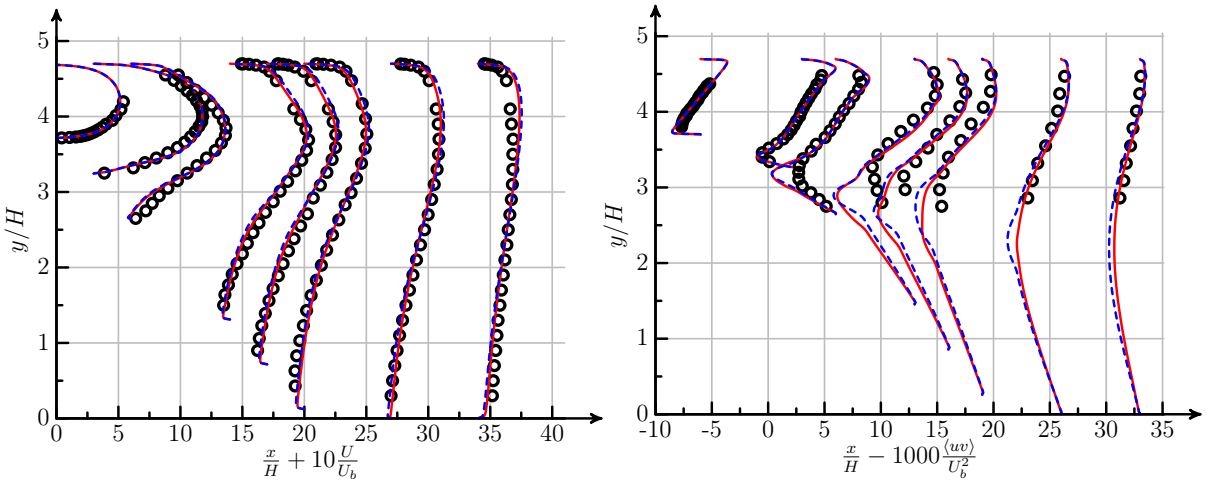

(**a**) Mean Velocity (**b**) Reynolds Stress

Figure 11: Computed results for a planar diffuser ($Re_H = 20{,}000$). Symbols, experimental data from Buice and Eaton[18]. Solid lines, computed results of standard SST model (Eqn. 2). Dashed lines, computed results of modified SST model (Eqn. 3).

5.3 Axisymmetric Transonic Bump

The final computational example is transonic flow over a circular arc, which leads to a shock wave and a steady separation bubble downstream of the shock (cf. Fig. 12a). This configuration was studied experimentally by Bachalo and Johnson[19]. Figure 12b presents the computed and experimental pressure coefficient along the wall. The extent of the experimental separation bubble is noted. The standard SST model is in close agreement with the experimental shock location despite discrepancies in the separated flow region. The modified diffusion model moves the shock location slightly upstream due to an increase in the extent of the computed separation bubble. The mean flow and turbulent velocity fluctuation data are presented in Fig. 13. In general, both the mean flow and turbulent predictions of the modified and standard SST model are poor. In contrast to the previous planar diffuser results, here both models significantly underpredict the Reynolds

stress in the separated flow region.

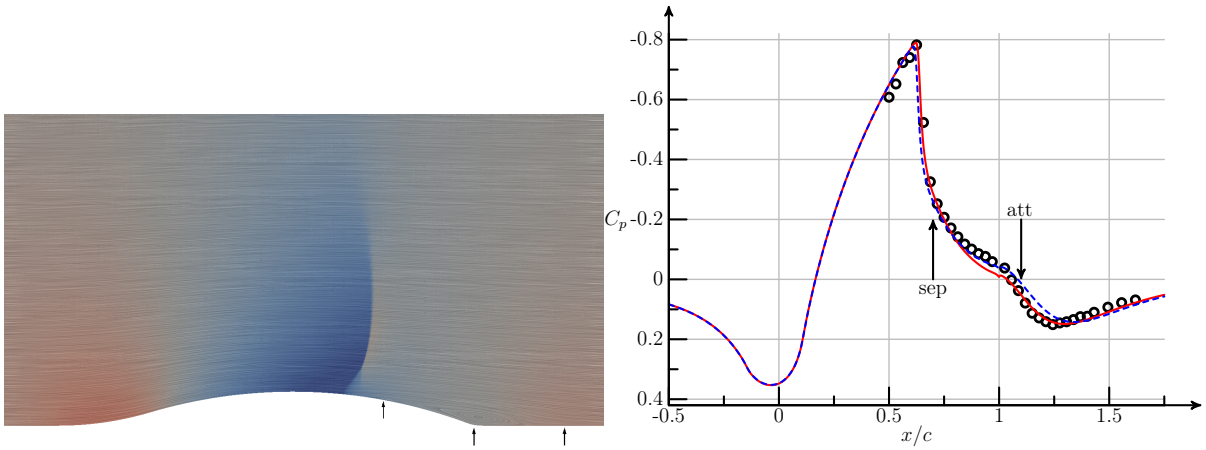

(**a**) Measurement Stations (**b**) Pressure Coefficient

Figure 12: Computed results for an axisymmetric transonic bump ($M_\infty = 0.875$, $Re_c = 131\text{x}10^3$). Flowfield colored by pressure coefficient and line-integral convolution of the velocity field for standard SST model (Eqn. 2). Experimental measurement stations noted by arrows. Symbols, experimental data from Bachalo and Johnson[19]. Solid lines, computed results of standard SST model (Eqn. 2). Dashed lines, computed results of modified SST model (Eqn. 3).

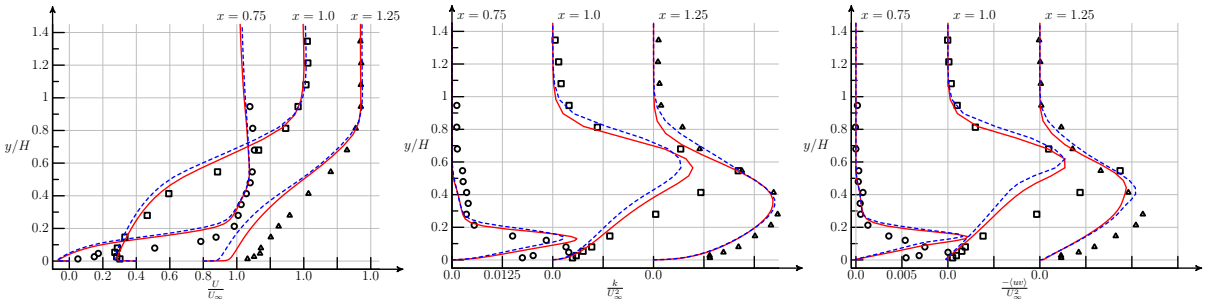

(**a**) Mean Velocity (**b**) Turb. Kinetic Energy (**c**) Reynolds Stress

Figure 13: Computed results for an axisymmetric transonic bump ($M_\infty = 0.875$, $Re_c = 131\text{x}10^3$). Symbols, experimental data from Bachalo and Johnson[19]. The experimental circumferential turbulent velocity fluctuation is assumed as $\langle ww \rangle = \frac{1}{2}\left(\langle uu \rangle + \langle vv \rangle\right)$. Solid lines, computed results of standard SST model (Eqn. 2). Dashed lines, computed results of modified SST model (Eqn. 3).

6 Summary

A suite of turbulence benchmark cases is a tool to understand trends in turbulence model predictions, rather than isolated datapoints. Examining the prediction of turbulence quantities, not just mean flow velocity or pressure data, provides a more sensitive measure of model performance and further illuminates the trends. To support the development and evaluation of next-generation turbulence models, a parallel effort to provide Direct Numerical Simulations (DNS) for many of the benchmark cases is underway. Similarly, an effort is underway to fully automate the application of this test suite for regression testing.

One trend examined here is the lack of sufficient diffusion at the edge of a free shear layer using the standard SST turbulence model. Empirical modifications of the diffusion coefficients of the standard SST turbulence model to increase the computed Reynolds stress at the edge of a shear-layer demonstrate improvements in the model predictions across a range of simulations. These modifications do not significantly degrade the calibration of the model for wall-bounded flows, or in the presence of an adverse pressure gradient.

Acknowledgments

Svetlana Poroseva of the University of New Mexico suggested the diffusion coefficients in the SST model as a topic of interest. Paul Stremel of Science and Technology Corp. at NASA Ames Research Center provided an initial prototype for scripting simulations within the turbulence modeling database.

References

[1] Bardina, J.E., Huang, P.G., and Coakley, T.J., "Turbulence Modeling Validation," AIAA Paper 97-2121, 1997.

[2] Nichols, R.H., Tramel, R.W., and Buning, P.G., "Solver and Turbulence Model Upgrades to OVERFLOW 2 for Unsteady and High-Speed Applications," AIAA Paper 2006-2824, 2006.

[3] Rumsey, C.L., Smith, B.R., Huang, G.P., "Description of a Website Resource for Turbulence Modeling Verification and Validation," AIAA Paper 2010-4742, June 2010.

[4] Childs, R.E., Garcia, J.A., Melton, J.E., Rogers, S.E., Shestopalov, A.J., and Vicker, D.J., "Overflow Simulation Guidelines for Orion Launch Abort Vehicle Aerodynamic Analyses," accepted for publication, AIAA 29th Applied Aerodynamics Conference, June 2011.

[5] Menter, F.R., "Two-Equation Eddy-Viscosity Turbulence Models for Engineering Applications," *AIAA Journal*, 32(8):1598–1605, 1994.

[6] Chan, W. M., Gomez, R.J., Rogers, S.E., and Buning, P.G., "Best Practices in Overset Grid Generation," AIAA Paper 2002-3191, June 2002.

[7] Hussein, H.J., Capp, S.P., and George, W.K., "Velocity measurements in a high-Reynolds-number, momentum-conserving, axisymmetric, turbulent jet," *Journal of Fluid Mechanics*, 258: 31–75, 1994.

[8] Poroseva, S.V. and Bézard, H., "On Ability of Standard k-ϵ Model to Simulate Aerodynamic Turbulent Flows," *Computational Fluid Dynamics Journal*, pp. 627–633, 2001.

[9] Cazalbou, J.B., Spalart, P.R., and Bradshaw, P., "On the behavior of two-equation models at the edge of a turbulent region," *Physics of Fluids*, 6(5):1797–1804, 1994.

[10] Bell, J.H. and Mehta, R.D., "Development of a Two-Stream Mixing Layer from Tripped and Untripped Boundary Layers," *AIAA Journal*, 28(12):2034–2042, 1990.

[11] Rogers, M.M. and Moser, R.D., "Direction simulation of a self-similar turbulent mixing layer," *Physics of Fluids*, 6:903–923, 1994.

[12] Gutmark, E. and Wygnanski, I., "The planar turbulent jet," *Journal of Fluid Mechanics*, 73(3): 465–495, 1976.

[13] Pope, S.B., "An Explanation of the Turbulent Round-Jet/Plane-Jet Anomaly," *AIAA Journal*, 16(3):279–281, 1978.

[14] Watson, R.D., Hall, R.M., and Anders, J.B., "Review of Skin Friction Measurements Including Recent High-Reynolds Number Results from NASA Langley NTF," AIAA Paper 2000-2392, June 2000.

[15] Eriksson, J.G., Karlsson, R.I., and Persson, J., "An experimental study of a two-dimensional plane turbulent wall jet," *Experiments in Fluids*, 25(1):50–60, 1998.

[16] Samuel, A.E. and Joubert, P.N., "A boundary lyaer developing in an increasingly adverse pressure gradient," *Journal of Fluid Mechanics*, 66(3):481–505, 1974.

[17] Menter, F.R., "Zonal Two Equation k-ω Turbulence Models for Aerodynamic Flows," AIAA Paper 93-2906, 1993.

[18] Buice, C.U. and Eaton, J.K., "Experimental Investigation of Flow Through an Asymmetric Plane Diffuser," *Journal of Fluids Engineering*, 122:433–435, 2000.

[19] Bachalo, W.D. and Johnson, D.A., "Transonic Turbulent Boundary-Layer Separation Generated on an Axisymmetric Flow Model," *AIAA Journal*, 24:437–443, 1986.